

An Angular Overlap Model for Cu(II) Ion in the AMOEBA Polarizable Force Field

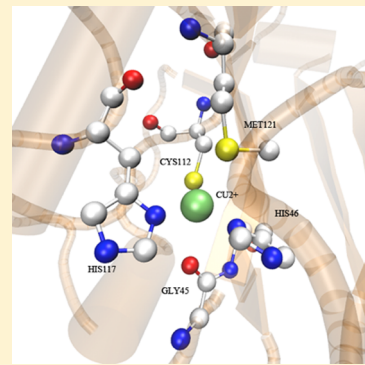
Jin Yu Xiang[†] and Jay W. Ponder*,‡

[†]Department of Biochemistry and Molecular Biophysics, Washington University in St. Louis, St. Louis, Missouri 63110, United States

[‡]Department of Chemistry, Washington University in St. Louis, St. Louis, Missouri 63130, United States

 Supporting Information

ABSTRACT: An extensible polarizable force field for transition-metal ions was developed based on AMOEBA and the angular overlap model (AOM) with consistent treatment of electrostatics for all atoms. Parameters were obtained by fitting molecular mechanics (MM) energies to various ab initio gas-phase calculations. The results of parametrization were presented for copper(II) ion ligated to water and model fragments of amino acid residues involved in the copper binding sites of type 1 copper proteins. Molecular dynamics (MD) simulations were performed on aqueous copper(II) ion at various temperatures as well as plastocyanin (1AG6) and azurin (1DYZ). Results demonstrated that the AMOEBA-AOM significantly improves the accuracy of classical MM in a number of test cases when compared to ab initio calculations. The Jahn-Teller distortion for hexa-aqua copper(II) complex was handled automatically without specifically designating axial and in-plane ligands. Analyses of MD trajectories resulted in a six-coordination first solvation shell for aqueous copper(II) ion and a 1.8 ns average residence time of water molecules. The ensemble average geometries of 1AG6 and 1DYZ copper binding sites were in general agreement with X-ray and previous computational studies.



INTRODUCTION

The d-block transition-metal (TM) ions play important catalytic and structural roles in a diverse range of organic and biomolecular systems due to the variety of d-shell chemistry.^{1–7} Being able to study these systems in silico can provide valuable insights to questions otherwise difficult to answer experimentally.^{8,9} However, quantum effects in the d-shell have proved to be a challenge for computational models of TM ions.¹⁰ Although TM ions can be treated as classical ions at long-range, the local ligand field effect as a result of interactions between ligand and TM ion can dramatically affect the properties of TM complexes.^{11,12} Currently, the most reliable methods to model TM ions are based on molecular orbital (MO) theory. TM systems are either entirely treated by ab initio quantum mechanics (QM), commonly based on functional density theory (DFT)^{13,14} and semiempirical MO methods,^{15,16} or partially through hybrid quantum mechanics/molecular mechanics (QM/MM) methods in which only a local region around TM ion is fully described by QM, while the rest of the system is treated by MM.¹⁷ Despite recent advances such as linear scaling electron correlation techniques,^{18,19} QM computations remain orders of magnitude more expensive in terms of computational cost than MM, and it is difficult to perform long time-scale simulations on large biomolecular systems using QM. On the other hand, MM calculations are very computationally efficient, but more studies are required to demonstrate that MM can achieve accuracies comparable to established QM methods.

A number of different MM models have been reported that describe TM-ligand interactions with varying degree of success. The simplest approach is by fitting traditional force field terms such as bonds, angles, and torsions to known properties obtained from experiments or QM calculations.⁸ However, the force field parameters fitted through this process generally have limited transferability and different parameters might be necessary for the same type of ligand depending on ligation geometry. More importantly, traditional angular potentials based on reference ligand–metal–ligand (L-M-L) values are inappropriate for describing TM complexes since the details of ligation geometries vary dynamically with overall ligand arrangements. A more radical solution is to construct a “reactive” model that allows atoms to respond chemically to their environment by dynamically assigning bond orders and charges based on molecular geometries.^{20,21} Alternatively, there are “semi-classical” models that employ potential functions for TM ions derived from the valence bond (VB) theory^{22–25} or the angular overlap model (AOM)²⁶ to supplement traditional force field energy terms. Models such as VALBOND^{27–30} are based on a simplified version of the VB theory, in which TM ions are treated as hypervalent resonance centers and L-M-L interactions are described by geometric overlap between sd^n hybridized bonding metal–ligand orbitals. On the other hand, models proposed by Deeth et al.^{31–33} and Carlsson et al.^{34–37} are developed from the AOM and the ligand field (LF) effects

Received: September 1, 2013

Published: November 18, 2013



ACS Publications

© 2013 American Chemical Society

are handled through explicit diagonalization of a perturbed d-orbital matrix due to the presence of ligands. These methods have demonstrated satisfactory agreements with experiments and ab initio calculations when used to study a range of TM systems with different coordination geometries and ligation states.

One of the main shortcomings of most implementations of semiclassical force fields is the lack of treatment on polarization, which is an important long-range energetic factor that needs to be incorporated when studying systems that involves highly polar sites.³⁸ We have previously proposed a polarizable TM force field model for aqueous Cu²⁺ and Zn²⁺ ions constructed upon atomic multipole optimized energetics for biomolecular applications (AMOEBA) and the VB theory.^{39,40} We found that the AMOEBA-VB model showed good agreement with numerous QM calculations and were able to reproduce aqueous ligation geometries within range of published experimental and computational results during molecular dynamics (MD) simulations. Nevertheless, the simple VB resonance weighting function used in the study did not readily handle the Jahn-Teller distortion in hexa-aqua Cu²⁺ complex, and generalizing the VB model to more complex systems has been challenging. In light of reports by Deeth et al. that the AOM approach can successfully describe the Jahn-Teller distortion and is extensible to wide range of TM complexes,^{10,41–43} we investigate the effectiveness of incorporating this alternative TM theory into the AMOEBA model. Furthermore, we seek to improve upon previous efforts by developing a model that has consistent electrostatic treatment for TM ion at all distances to allow the study of ligand dissociation and association.

In this report, we present an AOM for Cu²⁺ ion in the AMOEBA polarizable force field. In order to demonstrate the extensibility of the AOM approach, we study the accuracy of AMOEBA-AOM for both aqueous Cu²⁺ ion and type 1 blue copper (T1Cu) proteins. Specifically, plastocyanin (PDB: 1AG6)⁴⁴ and azurin (PDB: 1DYZ)⁴⁵ blue copper proteins, or cupredoxins, are electron transport proteins that shuttle electrons from donors to acceptors in bacteria and plants. This process takes advantage of the redox potential of Cu²⁺ and Cu⁺ ions. T1Cu proteins are chosen as validation targets because they are well-studied systems^{46–48} with binding sites that involve most of the common ligands for Cu²⁺ ion in biomolecules. In addition, high-resolution X-ray crystal structures are available for these proteins. It has been suggested that the electrostatic interactions are responsible for long-range molecular recognition of T1Cu proteins and the hydrophobic pocket near the copper binding site contributes to the precise docking of binding partners.⁴⁷ Therefore it is of interest to apply a force field model describing both the local coordination geometry and electrostatic properties of the copper binding sites when studying these proteins.

AMOEBA-AOM force field parameters are determined against a range of gas-phase QM calculations on metal complexes and validated against experimental data. In developing parameters for T1Cu proteins, small model fragments for protein side chains and backbones are used in QM routines. Energy evaluations on gas-phase metal complexes as well as results from MD simulations of aqueous Cu²⁺ ion and T1Cu proteins are reported.

METHODS

AMOEBA-AOM Framework. For a TM system, the total potential for the AMOEBA-AOM can be expressed as a sum of the general AMOEBA potential and the AOM energy terms specific for TM ions:

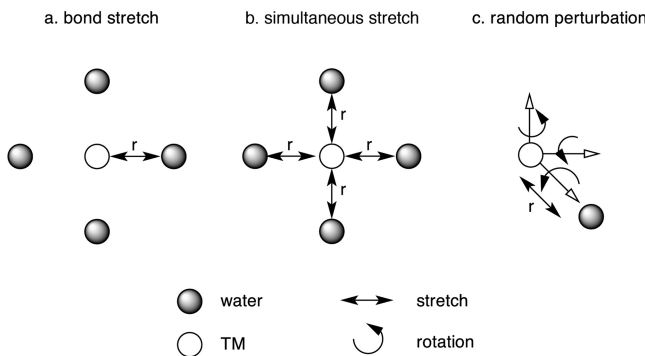


Figure 1. Routines for generating structural variants from QM-optimized aqua Cu²⁺ complexes for use in the AMOEBA-AOM parametrization process. (a) A single copper–water distance is varied, while other ligands retain their optimized coordinates. (b) All copper–water distances are changed simultaneously with each ligand equidistant from the copper ion. (c) Random perturbations were introduced by varying copper–water distances as well as by rotating the ligands with respect to the copper–oxygen vector and two axes orthogonal to the vector.

$$U_{\text{total}} = U_{\text{AMOEBA}} + U_{\text{AOM}} \quad (1)$$

where

$$\begin{aligned} U_{\text{AMOEBA}} = & U_{\text{bond}} + U_{\text{angle}} + U_{\text{b-a}} + U_{\text{oop}} + U_{\text{torsion}} + U_{\text{vdW}} \\ & + U_{\text{ele}}^{\text{pem}} + U_{\text{ele}}^{\text{ind}} \end{aligned} \quad (2)$$

The first five terms of eq 2 are valence contributions representing bond stretch, angle bend, bond-angle cross-term, out-of-plane bond, and torsional rotation, respectively. The last three terms are nonbonded intermolecular energy terms, including the van de Waals (vdW), permanent electrostatic, and induced electrostatic potentials.^{39,49,50}

AMOEBA Potentials. The details of the AMOEBA model have been previously reported.^{39,49,50} For TM complexes, only nonbonded energy terms are applied between the metal and its ligands. This is similar to the treatment of other main group cations with the exception that the AOM bonding terms are used between metal ions and the atoms that are directly ligated instead of the normal vdW terms. The vdW interactions take the form of a buffered 14-7 potential as described by Halgren:⁵¹

$$U_{ij}^{\text{vdW}} = \epsilon_{ij} \left(\frac{1 + \delta}{\rho_{ij} + \delta} \right)^{n-m} \left(\frac{1 + \gamma}{\rho_{ij}^m + \gamma} - 2 \right) \quad (3)$$

where $\rho_{ij} = R_{ij}/R_{ij}^0$, $n = 14$, $m = 7$, $\delta = 0.07$, and $\gamma = 0.12$. ϵ_{ij} and R_{ij}^0 represent the potential energy well-depth, minimum energy distance and the separation between atoms i and j , respectively. Mixing rules are applied to ϵ_{ij} and R_{ij}^0 for heterogeneous atom pairs:

$$R_{ij}^0 \frac{(R_{ii}^0)^3 + (R_{jj}^0)^3}{(R_{ii}^0)^2 + (R_{jj}^0)^2} \quad (4)$$

$$\epsilon_{ij} = \frac{4\epsilon_{ii}\epsilon_{jj}}{(\epsilon_{ii}^{1/2} + \epsilon_{jj}^{1/2})^2} \quad (5)$$

As described below, for some ligand atom types, R_{ii}^0 is dynamically reduced via a cubic spline that is a function of ligand atom distances to the metal ion (r_{ML}):

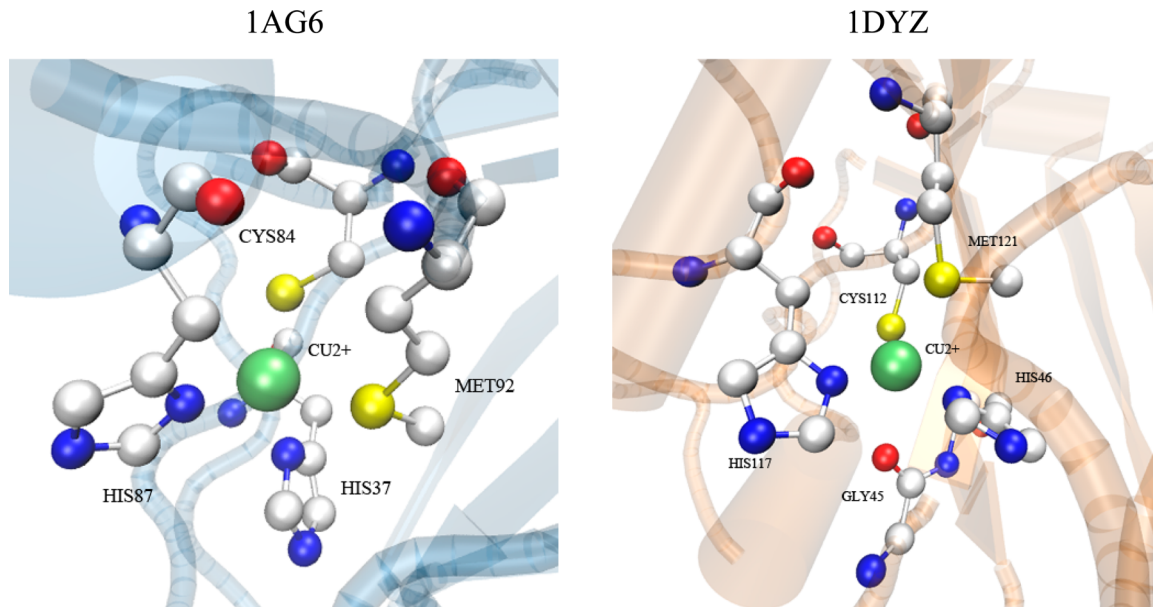


Figure 2. Visual representations of Cu^{2+} binding sites in X-ray structures of 1AG6 and 1DYZ. Colors: Cu^{2+} = lime green, oxygen = red, nitrogen = blue, sulfur = yellow, carbon = white.

$$R_{ii}^0 = R_{ii}^{0'} - (R_{ii}^{0'} - R_{ii}^{0''})a_{ii}$$

$$a = c_5 r_{ML}^5 + c_4 r_{ML}^4 + c_3 r_{ML}^3 + c_2 r_{ML}^2 + c_1 r_{ML} + c_0 \quad (6)$$

$R_{ii}^{0'}$ is the value for minimum energy distance at metal–ligand separation beyond r_{ML}^{\max} , while $R_{ii}^{0''}$ denotes the value at short-range ($< r_{ML}^{\min}$). This adjustment is needed to account for the reduction in atom size due to the polarization of ligand atoms toward the TM ion. The cubic spline ensures a smooth transition of R_{ii}^0 between r_{ML}^{\max} and r_{ML}^{\min} . The coefficients for the function are determined by imposing boundary conditions such that the dimensionless scaling factor a is 0 at r_{ML}^{\max} and 1 at r_{ML}^{\min} , while the first and second derivatives are 0 at r_{ML}^{\max} and r_{ML}^{\min} :

$$c_5 = -6/\tau$$

$$c_4 = 15(r_{ML}^{\max} + r_{ML}^{\min})/\tau$$

$$c_3 = -10(r_{ML}^{\max 2} + 4r_{ML}^{\max}r_{ML}^{\min} + r_{ML}^{\min 2})/\tau$$

$$c_2 = 30(r_{ML}^{\max 2}r_{ML}^{\min} + r_{ML}^{\max}r_{ML}^{\min 2})/\tau$$

$$c_1 = -30(r_{ML}^{\max 2}r_{ML}^{\min 2})/\tau$$

$$c_0 = r_{ML}^{\max 3}(r_{ML}^{\max 2} - 5r_{ML}^{\max}r_{ML}^{\min} + 10r_{ML}^{\min 2})/\tau$$

$$\tau = (r_{ML}^{\max} - r_{ML}^{\min})^5 \quad (7)$$

The electrostatic potential consists of a permanent and an induced component. The permanent contribution is described by atom-centered monopole, dipole, and quadrupole moments whose values are determined via Stone's distributed multipole analysis⁵² followed by refinement against QM-derived electrostatic potentials. Polarization is handled through self-consistent induced dipole, with a Thole damping factor applied at short interaction distances. This mechanism has a charge smearing effect that avoids the well-known polarization catastrophe at close separations.⁵³

AOM Potentials. The complete derivations of the AOM potentials for d-row TM ion have been published elsewhere.^{31,54} Here we reproduce the basic theory and its outcomes, along with modifications in the context of AMOEBA-AOM. Consider

Table 1. Corresponding Model Fragments Used in QM Gas-Phase Calculations to Model Copper Binding Sites of T1Cu Proteins

Binding site ligands	Model compound
Backbone carbonyl	
Histidine side chain	
Methionine side chain	
Cysteine side chain (deprotonated)	

a perturbing potential v^{LF} due to the presence of ligands. Its effect on the d-orbital energies of TM ion can be computed by first-order perturbation theory:

$$V_{ab}^{\text{LF}} = \langle d_a | v^{\text{LF}} | d_b \rangle \quad (8)$$

The AOM makes the approximation that the ligands contribute linearly to v^{LF} and that V_{λ}^{LF} is diagonal in the local frame of ligand λ , where the z-axis points away from the metal center toward the ligand atom:

$$\langle d_{\lambda,z^2} | v_{\lambda}^{\text{LF}} | d_{\lambda,z^2} \rangle = e_{\sigma} = e_1$$

$$\langle d_{\lambda,xz} | v_{\lambda}^{\text{LF}} | d_{\lambda,xz} \rangle = e_{\pi x} = e_2$$

$$\langle d_{\lambda,yz} | v_{\lambda}^{\text{LF}} | d_{\lambda,yz} \rangle = e_{\pi y} = e_3$$

$$\langle d_{\lambda,x^2-y^2} | v_{\lambda}^{\text{LF}} | d_{\lambda,x^2-y^2} \rangle = e_{\delta x^2-y^2} = e_4$$

$$\langle d_{\lambda,xy} | v_{\lambda}^{\text{LF}} | d_{\lambda,xy} \rangle = e_{\delta xy} = e_5 \quad (9)$$

For systems involving σ , πx and πy bondings, e_4 and e_5 can be set to zero. The orbital $|d_a\rangle$ ($a = 1-5$) can be expressed as a

radial function multiplied by real, $l = 2$ spherical harmonics d_i . In order to develop the angular potential for the ligands, we represent the angular components of $|d_a\rangle$ as

$$\mathbf{d} = \begin{pmatrix} d_1 \\ d_2 \\ d_3 \\ d_4 \\ d_5 \end{pmatrix} = \begin{pmatrix} d_z^2 \\ d_{xz} \\ d_{yz} \\ d_{x^2-y^2} \\ d_{xy} \end{pmatrix} = \begin{pmatrix} 0 & 0 & 1 & 0 & 0 \\ 0 & -1/\sqrt{2} & 0 & 1/\sqrt{2} & 0 \\ 0 & i/\sqrt{2} & 0 & i/\sqrt{2} & 0 \\ 1/\sqrt{2} & 0 & 0 & 0 & 1/\sqrt{2} \\ -i/\sqrt{2} & 0 & 0 & 0 & i/\sqrt{2} \end{pmatrix} \begin{pmatrix} Y_{22}(\hat{\mathbf{r}}) \\ Y_{21}(\hat{\mathbf{r}}) \\ Y_{20}(\hat{\mathbf{r}}) \\ Y_{2,-1}(\hat{\mathbf{r}}) \\ Y_{2,-2}(\hat{\mathbf{r}}) \end{pmatrix} \quad (10)$$

The local LF matrix must then be rotated into the global molecular frame. The spherical harmonics under the a rotation R can be written as

$$RY_{lm}(\hat{\mathbf{r}}) = \sum_{m'} D_{m'm}^l(\alpha\beta\gamma) Y_{lm}(\hat{\mathbf{r}}) \quad (11)$$

where α , β , and γ are Euler angles as defined in Rose.⁵⁵ For σ bonding, we can conveniently define local x -axis pointing away from the global z -axis, yielding

$$\alpha = 0, \quad \beta = -\theta, \quad \gamma = -\phi \quad (12)$$

for a ligand with polar coordinates r , θ , and ϕ . In the case of nonzero πx and πy bondings, the xz -plane should be in-plane with the planar ligand group. This necessitates an extra rotation through ψ , which is the angle between the new local x -axis and the one defined for σ bonding.⁵⁴ Hence:

$$\alpha = -\psi, \quad \beta = -\theta, \quad \gamma = -\phi \quad (13)$$

Rewriting eq 11 in matrix form \mathbf{D}_λ , the local \mathbf{y}_λ can be related to the global \mathbf{y} by:

$$\mathbf{y}^T = \mathbf{y}_\lambda^T \mathbf{D}_\lambda \quad (14)$$

Likewise,

$$\begin{aligned} \mathbf{d}_\lambda^T &= \mathbf{d}^T \mathbf{F}_\lambda \\ \mathbf{F}_\lambda &= \mathbf{C}^* \mathbf{D}_\lambda^\dagger \mathbf{C}^T \end{aligned} \quad (15)$$

taking advantage the fact that \mathbf{C} is unitary. From there we arrive at the expression:

$$\begin{aligned} \mathbf{V}^{LF} &= \sum_\lambda \mathbf{F}_\lambda \mathbf{E}_\lambda \mathbf{F}_\lambda^\dagger \\ E_{\lambda,ab} &= e_a \delta_{ab} \end{aligned} \quad (16)$$

If there is significant d-s hybridization, one must consider a 6×6 LF matrix involving perturbation by the $(n+1)s$ orbital. However, Deeth et al.³¹ has shown that the additional contribution can be simplified as

$$b_a = \sum_\lambda F_{\lambda,a} \sqrt{e_{ds}} \quad (17)$$

when taking into account the fact that only $|d_{\lambda,z^2}\rangle$ can have significant overlap with $|d_{\lambda,s}\rangle$. We can now construct the overall formulation as

$$\mathbf{V}^{LF} = \mathbf{V}^\sigma + \mathbf{V}^{\pi x} + \mathbf{V}^{\pi y} - \mathbf{b} \mathbf{b}^T \quad (18)$$

Diagonalizing the symmetric \mathbf{V}^{LF} results in energy eigenvalues w_a . Finally, combining with the occupancy of the levels (n_a), we arrive at the angular potential:

$$U_{AOM}^{\text{angle}} = \sum_a n_a w_a \quad (19)$$

In this initial iteration, a simple exponential function is used in AMOEBA-AOM for e_σ , $e_{\pi x}$, $e_{\pi y}$, and e_{ds} :

$$e_{AOM} = a_{AOM} r_{ML}^{-6} \quad (20)$$

AMOEBA-AOM differs from other implementations of similar models in MM force field³³ in that the classical electrostatic model is applied consistently to both the TM and its ligands. This setup allows the study of ligand exchanges since the AOM energy terms drops off rapidly with increasing metal-ligand separation, but electrostatic contributions remain significant at distances beyond ligation shell. It should be noted that retaining the electrostatic model affects the parametrization of a_{AOM} and therefore our parameter is not directly comparable with previously reported values.

The metal-ligand bonding interaction is described by a Morse potential:

$$U_{AOM}^{\text{bond}} = D(1 - e^{-a_{Morse}(r_{ML} - r_{ML,0})^2}) - D \quad (21)$$

where D , a_{Morse} , and $r_{ML,0}$ controls the bond strength, width of the potential well, and the minimum energy distance, respectively.

Parameterization and Validation. The AMOEBA-AOM parameters were determined via methods similar to previously published parametrization routines for the AMOEBA-VB model.⁴⁰ The general strategy was to fit the MM results of energy evaluations and geometry optimizations to those obtained by QM calculations on gas-phase TM complexes under a variety of different conditions. The AOM parameters were determined after the AMOEBA parameters had been obtained following the usual protocol.⁵⁰ The goal of the parametrization process is to obtain a single set of AOM parameters that best reproduces the QM results for all the test routines. Finally, analyses based on MD simulations were validated against available experimental and computational data.

All ab initio calculations were carried out with the Gaussian 09⁵⁶ software. Geometry optimization of aqua Cu^{2+} complexes were performed at the B3LYP/6-311G(d,p)⁵⁷⁻⁵⁹ level of theory. Single-point energies were evaluated by the MP2 electron correlation method,⁶⁰ with the aug-cc-pVTZ⁶¹ basis set on main group atoms and the cc-pVTZ⁶² on Cu^{2+} ion. A Fermi-broadening SCF technique⁶³ was used to improve convergence stability, and a relatively stringent SCF convergence criterion of 10^{-9} au was imposed. In the case of model complexes for the copper binding sites in T1Cu proteins, B2PLYP-D/cc-pVDZ^{64,65} and MP2/cc-pVDZ were utilized for geometry optimizations and for single-point energy calculations, respectively. Ligand internal coordinates were frozen during optimization calculations to increase computational efficiency. The AMOEBA-AOM energy terms and their corresponding analytical derivatives were implemented in the TINKER³⁹ MM package.

Gas-Phase Calculations on Aqua Cu^{2+} Complexes. The AMOEBA water parameters have been reported previously⁴⁹ and were unmodified for use with AMOEBA-AOM. QM geometry optimizations were performed on gas-phase tetra-aqua and hexa-aqua Cu^{2+} complexes under angular constraints to yield idealized square-planar, tetrahedral, and octahedral structures. The following procedures were used to compare MM and QM calculations performed on geometric variants generated from these optimized complexes:

- (1) Copper–water bonding potential curves were produced for square-planar $[\text{Cu}(\text{H}_2\text{O})_4]^{2+}$ and octahedral $[\text{Cu}(\text{H}_2\text{O})_6]^{2+}$ by performing single-point energy evaluations at varying copper–oxygen distances for a single water molecule. Axial and in-plane water molecules in $[\text{Cu}(\text{H}_2\text{O})_6]^{2+}$ are monitored separately to illustrate the effect of the Jahn–Teller distortion. Zero energy is taken to be the potential of complex with copper–oxygen distance at 5 Å. Total BSSE-corrected interaction energies for the complexes were also computed.
- (2) The potential energy difference between square-planar and tetrahedral $[\text{Cu}(\text{H}_2\text{O})_4]^{2+}$ is plotted as a function of copper–oxygen separations, with water–water interactions removed. This gives a direct measurement to the LF effect since it is known that four-coordinated Cu^{2+} complexes do not adopt the tetrahedral geometry for small ligands, which minimizes water–water repulsion.^{8,12,36}
- (3) One hundred complex structures were generated by introducing small geometric perturbations to the optimized square-planar $[\text{Cu}(\text{H}_2\text{O})_4]^{2+}$ and octahedral $[\text{Cu}(\text{H}_2\text{O})_6]^{2+}$. This process involves randomly perturbing

copper–oxygen distance by a maximum of ± 0.35 Å deviation from optimal value as well as rotating each of the water molecules around the copper–oxygen vector and two orthogonal axes between 0 and 10°. Structures with water–water separation < 2.5 Å were discarded. MM computed energies for these complexes were compared to the results obtained from QM to investigate whether MM models can reproduce the QM energy surface near the optimum geometry. Structures with QM energies more than 30 kcal/mol higher than that of the idealized geometry were discarded since these high-energy structures are not readily accessible during routine MD simulations.

Procedural diagrams for routines described above are available in Figure 1.

Gas-Phase Calculations on Model Complexes for Cu^{2+} Binding Sites in T1Cu Proteins. The Cu^{2+} binding site of 1AG6 plastocyanin consists of two histidine, one cysteine, and one methionine residue.⁴⁴ In addition to these ligands, the copper ion is coordinated by an extra backbone carbonyl oxygen in the structure of 1DYZ azurin.⁴⁵ The structures of the Cu^{2+} binding sites are visualized in Figure 2. For gas-phase calculations performed during the AOM parametrization process, complete amino acid residues were substituted by small model compounds, which were chosen to maintain similar ligand properties. The identities of the corresponding model fragments can be found in Table 1. For the sake of brevity, the model complexes for 1AG6 and 1DYZ Cu^{2+} binding sites will be denoted by T1Cu1 and T1Cu2, respectively, in the following discussions. The AMOEBA parameters for the ligands were obtained following the published protocol, and their values can

Table 2. AOM Parameters for Water, T1Cu1, and T1Cu2 Ligands Defined by the Bolded Atoms^a

Ligand	H-O-H				
a_{σ}	110	13811	494	6269	5360
a_{ds}	90	2170	4	793	1664
$a_{\pi\pi}$	0	1200	0	0	265
$a_{\pi\rho}$	5	1200	106	132	265
D	1.160	130.0	10.00	18.00	1.00
a_{Morse}	1.810	3.950	1.750	2.900	1.000
$r_{\text{ML},0}$	2.835	2.200	2.500	2.800	4.000
$R_i^{0\prime}$	1.703	1.650	1.855	2.000	2.175
$R_i^{0\prime\prime}$	1.703	1.650	1.705	1.950	2.000

^aSee eqs 6, 20, and 21 for variable definitions. Ligands with the same value of $R_i^{0\prime}$ and $R_i^{0\prime\prime}$ indicate that vdw scaling is not applied. r_{ML}^{\min} and r_{ML}^{\max} are set at 4.5 and 6 Å, respectively, for all ligands.

Table 3. Comparison between BSSE-Corrected QM and AMOEBA-AOM Interaction Energies of Single Water Molecule with the Rest of Gas-Phase Aqua Cu^{2+} Complex^a

	QM (BSSE)	AMOEBA-AOM
$[\text{Cu}(\text{H}_2\text{O})_4]^{2+}$	-48.16 (1.10)	-44.61
$[\text{Cu}(\text{H}_2\text{O})_4]^{2+}$ (axial)	-25.52 (0.90)	-30.38
$[\text{Cu}(\text{H}_2\text{O})_4]^{2+}$ (in-plane)	-30.08 (1.33)	-33.18

^aUnits in kcal/mol.

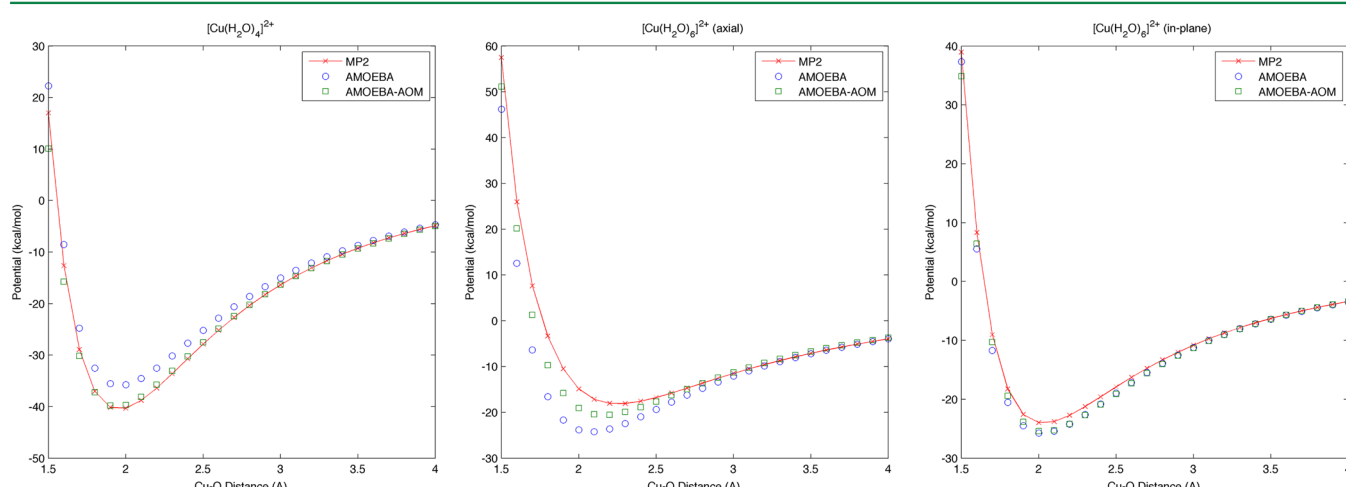


Figure 3. Bonding potential curve of water molecule generated using QM and MM methods. Zero bonding potential energy is taken as the potential of the complex with a water molecule at 5 Å.

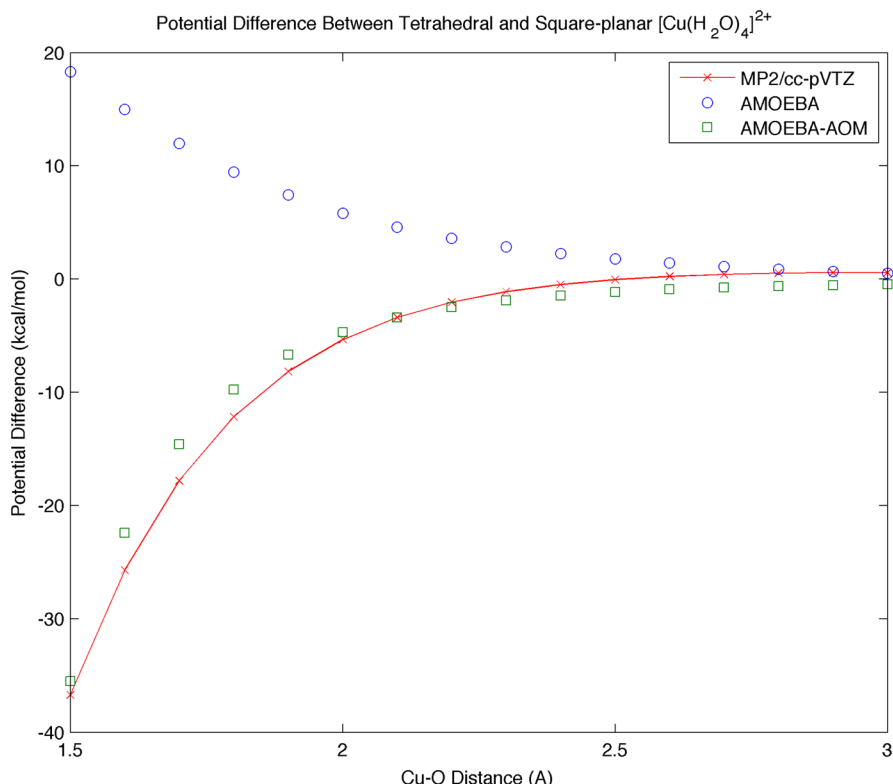


Figure 4. Potential energy difference between square-planar and tetrahedral tetra-aqua Cu^{2+} complexes with the water–water interaction removed. Negative values indicate that the square-planar structure is lower in potential energy than the tetrahedral geometry.

be found in the Supporting Information. Similar to water molecules, the AOM parameters were obtained by fitting results from a series of MM computations to that obtained from QM:

- (1) Geometry optimizations were carried out for T1Cu1 and T1Cu2 using both QM and MM. The ligation geometries of the optimized structures were compared.
- (2) QM binding energies are computed by performing counterpoise-corrected MP2 calculations on B2PLYP-D optimized structures with the ligand and the rest of the complex in two different fragments. The data are then compared to MM interaction energies that are calculated by subtracting potentials of individual ligand and the remaining molecules from the overall complex energy.
- (3) Random complex structures were generated for T1Cu1 and T1Cu2 following similar routines to that applied to aqua Cu^{2+} complexes. The ligand molecules are rotated from QM optimized geometry by a maximum of 15° with respect to metal–ligand vector, defined by the Cu^{2+} ion and atom directly ligated to the metal and two orthogonal axes. A minimum ligand–ligand contact distance of 2.5 \AA is maintained. Sets of 100 structures were generated for each ligand, and only a single ligand is perturbed within each set. Geometries with ab initio energy higher than 5 kcal/mol from the QM optimized complexes were discarded when comparing QM and MM potentials.

Aqueous Cu^{2+} Ion Simulations. Canonical ensemble MD simulations were performed on a single Cu^{2+} ion solvated in a 18.6215 \AA cubic water box. Period boundary condition was enforced, and particle-mesh Ewald summation was applied to long-range electrostatic interactions.^{66,67} Self-consistent dipole polarization was converged to 0.01 D root-mean-squared

(RMS) change in atomic induced dipole moments. Multiple 80 ns trajectories taken at 1 fs time-step were collected at 0.1 ps interval with simulation temperature set at $298, 320, 350$, and 380 K . The correlation function, solvation shell properties, coordination numbers, and average water residence times in the first solvation shell were calculated from each of the trajectories and compared against previous published data. The first 100 ps of the trajectories were discarded to allow for system equilibration. Shorter 8 ns simulations were also performed with a 30 \AA solvation cube under the same simulation conditions to verify that the finite periodic box size did not affect the observations obtained.

T1Cu Proteins Simulations. MD simulations were carried out at 298 K in the canonical ensemble for 1AG6 and 1DYZ proteins. The available AMOEBA protein parameters (parameter file: amoebabio09.prm) were used,⁶⁸ while the AMOEBA-AOM parameters derived from T1Cu1 and T1Cu2 were applied to the appropriate residues. Water molecules external to the proteins were first removed from the X-ray structures. Hydrogen atoms were then added, with positions determined from heavy-atom bonding geometries. The protonation state of histidine residues is assigned by analyzing the local hydrogen-bonding network.⁶⁹ Additionally, unresolved atoms were filled in manually to construct a full side chain for GLU19 of 1DYZ. The protein structures were solvated in water inside a 98.6726 \AA truncated octahedron. Before simulations were conducted, the water molecules coordinates were minimized to 3 kcal/mol RMS change in potential energy gradient, followed by minimization on the entire system to 2 kcal/mol . Settings for dipole polarization and long-range electrostatics were identical to that used in simulations for aqueous Cu^{2+} and periodic boundary condition was applied. A total of 2 ns of MD trajectories were collected for each protein. The geometries of Cu^{2+} binding sites

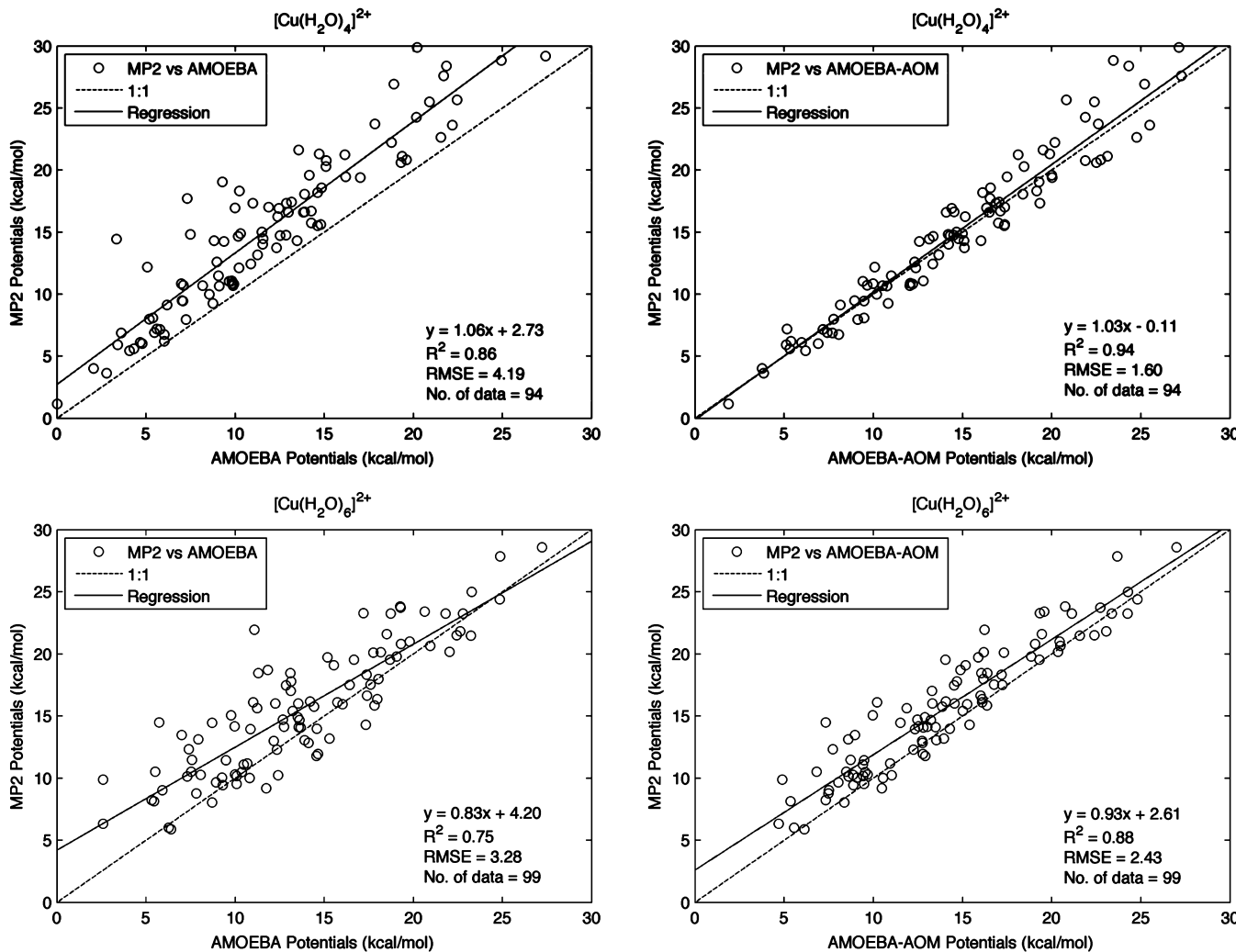


Figure 5. Comparisons between QM and MM potentials of random aqua Cu²⁺ complexes generated by perturbing the QM-optimized structure.

were compared against previously published experimental and computational studies.

RESULTS AND DISCUSSIONS

AMOEBA-AOM Parameters. The AMOEBA parameters for Cu²⁺ ion are identical to those used in our previous AMOEBA-VB study.⁴⁰ The AOM parameters for water, T1Cu1, and T1Cu2 ligands are presented in Table 2. A number of constraints on the values of the AOM parameters are applied during the parametrization process. First, e_{σ} should be the largest contribution to the AOM matrix, since it represents the principle LF. Second, the $e_{\pi x}$ term is zero for ligand atoms with two bonded subsidiary atoms, as the local y -axis is taken to be perpendicular to the ligand plane. Finally, $e_{\pi x}$ and $e_{\pi y}$ have equal values in the case of ligand atoms with a single bonded subsidiary atom because the contributions from ligand orbitals should be cylindrical. A common set of AOM parameters was used in all the calculations presented in this report.

Water. Gas-Phase Calculations on Aqua Cu²⁺ Complexes. The bonding potentials of water molecules for square-planar [Cu(H₂O)₄]²⁺ and octahedral [Cu(H₂O)₆]²⁺ are plotted in Figure 3. Both AMOEBA and AMOEBA-AOM can reproduce the QM minimum energy distance for [Cu(H₂O)₄]²⁺, but AMOEBA underestimates the strength of interaction by 4.5 kcal/mol, whereas AMOEBA-AOM (-39.8 kcal/mol) is

in better agreement with QM results (-40.3 kcal/mol). For [Cu(H₂O)₆]²⁺, data from AMOEBA and AMOEBA-AOM are comparable for in-plane water molecules. However, AMOEBA is not able to capture the distortion of axial water molecules, while AMOEBA-AOM can reasonably describe the structural extent of the Jahn-Teller distortion. The QM-derived bonding distance for an axial water is 2.3 Å, compared to 2.1 and 2.2 Å for AMOEBA and AMOEBA-AOM, respectively. In addition, AMOEBA-AOM (-20.5 kcal/mol) produces binding energy closer to that of QM (-18.0 kcal/mol) than AMOEBA (-24.2 kcal/mol). A comparison of BSSE-corrected QM interaction energy of single water molecule with the rest of the complex to that computed by AMOEBA-AOM is tabulated in Table 3.

Figure 4 shows the potential energy differences between square-planar and tetrahedral [Cu(H₂O)₄]²⁺ complexes at varying copper–oxygen distances. It is evident that without the AOM terms, AMOEBA produces the wrong geometric preference for [Cu(H₂O)₄]²⁺. The AMOEBA-AOM model correctly prefers the square-planar geometry, and the computed energy difference is in good agreement with the QM results.

Figure 5 compares the QM and MM computed energy surfaces near the optimized square-planar [Cu(H₂O)₄]²⁺ and octahedral [Cu(H₂O)₆]²⁺. All the values presented are relative to the potential of the idealized structures. The addition of the AOM terms again dramatically improves the agreement

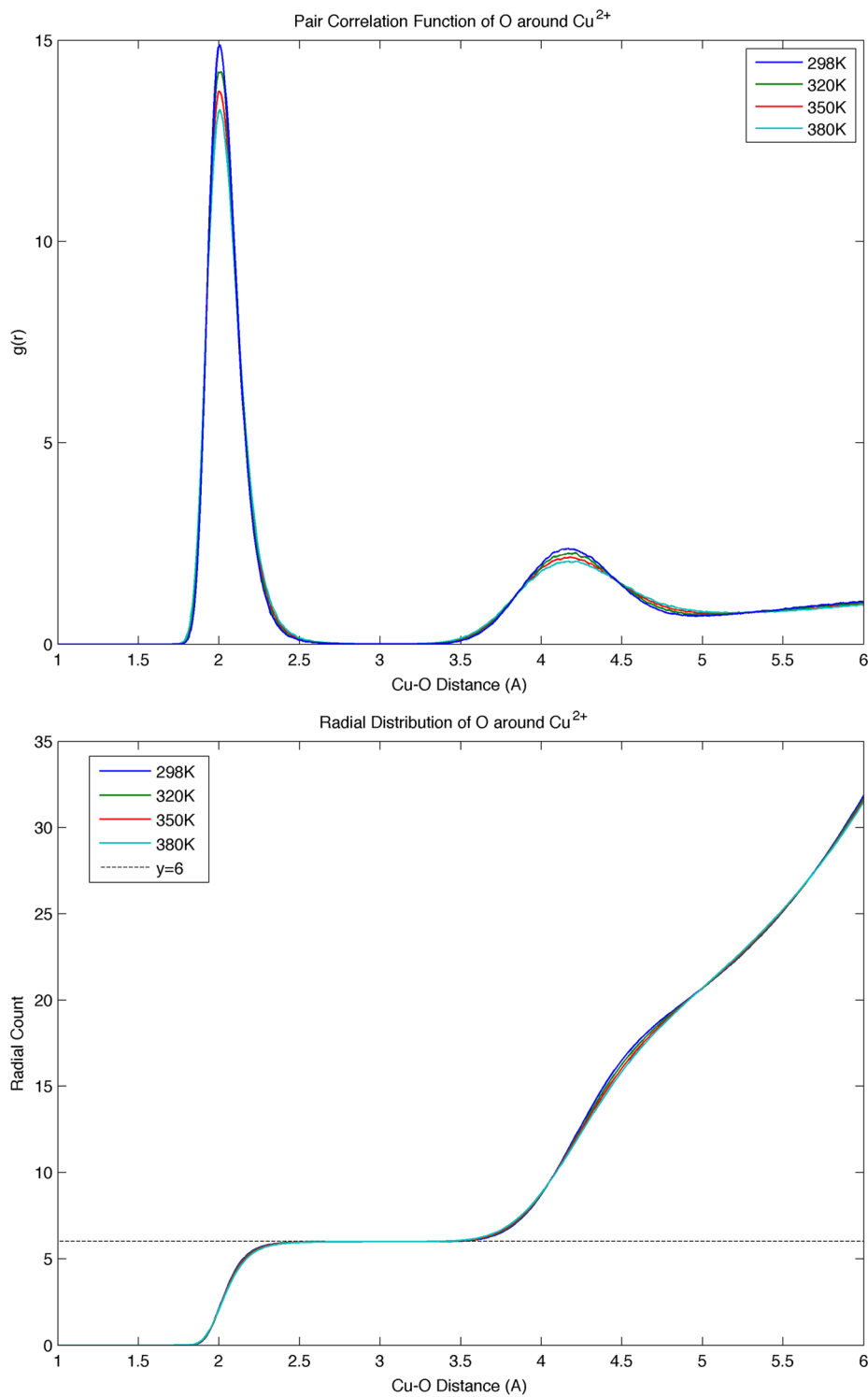


Figure 6. Copper–oxygen radial pairwise correlation (above) and distribution function (below) computed for MD trajectories at various simulation temperatures.

between QM and MM. The RMS deviation improves by 64% and 26% for $[\text{Cu}(\text{H}_2\text{O})_4]^{2+}$ and $[\text{Cu}(\text{H}_2\text{O})_6]^{2+}$, respectively. It is quite respectable that the AMOEBA-AOM model maintains good performance even for conformers that are close to 30 kcal/mol higher in energy than the optimized structure.

Aqueous Cu²⁺ Ion Simulations. The copper–oxygen pairwise correlation function and radial distribution are computed from MD simulations performed at 298, 320, 350, and 380 K (Figure 6). The occupancy of Cu²⁺ ion first solvation shell has

been a controversial topic. Various coordination numbers ranging from 5 to 6 have been reported by experimental and computational studies.^{70–77} Other studies suggested that both five- and six-coordination structures dynamically exchange in aqueous Cu²⁺⁷⁸ and that coordination number can be temperature dependent.⁷¹ The radial distribution obtained from our calculations suggests a predominant six-coordinate first solvation shell at all simulation temperatures. This result echoes the observations we made in our previous study on aqueous

Cu^{2+} ion using the AMOEBA-VB model.⁴⁰ The lower peak value of the correlation function at higher temperatures indicates a less-structured solvation shell. In addition, we are unable to observe the “dual-peak” character previously obtained from simulation carried out with ReaxFF model.²¹ The results remain the same when performing the analysis on shorter segments of the trajectories that mimics the simulation length of previous study. We have also verified that the results remain unchanged when the simulations were repeated with larger 30 Å cubic box, indicating that the observations are not affected by the finite periodic condition. A summary of comparisons on the coordination geometries taken from present and prior reports can be found in Table 4. It is interesting that the AMOEBA-AOM model is able to describe the Jahn–Teller distortion as observed in gas-phase calculations. But the aqueous coordination

of Cu^{2+} ion seems to be dominated by the space-filling effect of water molecules in our simulations. Another possible explanation for the lack of five-coordinate species in our simulation is that these are transient structures with lifetimes in the femtosecond time scale, which is shorter than the 0.1 ps resolution of our collected data.

Previous O¹⁸ NMR studies have reported the average residence times of water molecules in the first solvation shell is ~ 5 ns.^{72,79,80} However, this value is subject to considerable uncertainty due to the deficiency in the quality of spin relaxation data that the octahedral coordination model was fitted to. In our simulation, the lifetime of water molecules in the first solvation shell is computed by tabulating the amount of continuous time a particular water oxygen atom spends within 3.2 Å to the Cu^{2+} ion. This cutoff distance is determined by inspecting the midpoint separation of first and second solvation shell as indicated in the Cu^{2+} –O pairwise correlation function (Figure 6). A short tolerance is allowed when a water molecule transiently moves in and out of the cutoff distance for noise filtering. The relationship between the computed residence times and the tolerance values is plotted in Figure 7. Depending on the aggressiveness of noise filtering, we obtained an average residence time of 0.6–1.8 ns at room temperature, which is in general agreement with experiments. As points of reference, the computed water residence time for Cu^{2+} is much shorter than previously reported room-temperature experimental values for other third-row TM ions Ni^{2+} (37 μs) and Fe^{2+} (0.3 μs) but longer than Zn^{2+} (0.1–5 ns).^{72,81} Finally, we expectedly observed a trend of shortening of residence times with increasing simulation temperature.

T1Cu Proteins. Gas-Phase Calculations on T1Cu1 and T1Cu2. Table 5 summarizes the geometries of optimized T1Cu1 and T1Cu2 structures using QM and MM. A visual

Table 4. First Solvation Shell Coordination Geometry of the Aqueous Cu^{2+} Ion^a

method	first solvation shell M–O coordination number and geometry	ref
MD (AMOEBA-AOM)	6×2.005	present work
MD (AMOEBA-VB)	6×2.005	40
MD (REAX-FF)	$4 \times 1.94 + 2 \times 2.27$	21
neutron diffraction	6×1.97	82
neutron diffraction	5×1.96	71
EXAFS	$4 \times 1.96 + 2 \times 2.60$	83
EXAFS	$4 \times 2.04 + 2 \times 2.29$	84
Car–Parrinello MD	5×1.96	71
Car–Parrinello MD	$4 \times 2.00 + 1 \times 2.45$	85
QM/MM	$4 \times 2.02 + 2 \times 2.29$	86
QM charge field MD	$4 \times 2.06 + 2 \times 2.21$	87

^aValue for the present work is taken from the first peak of the copper–oxygen pairwise correlation function generated at 298 K.

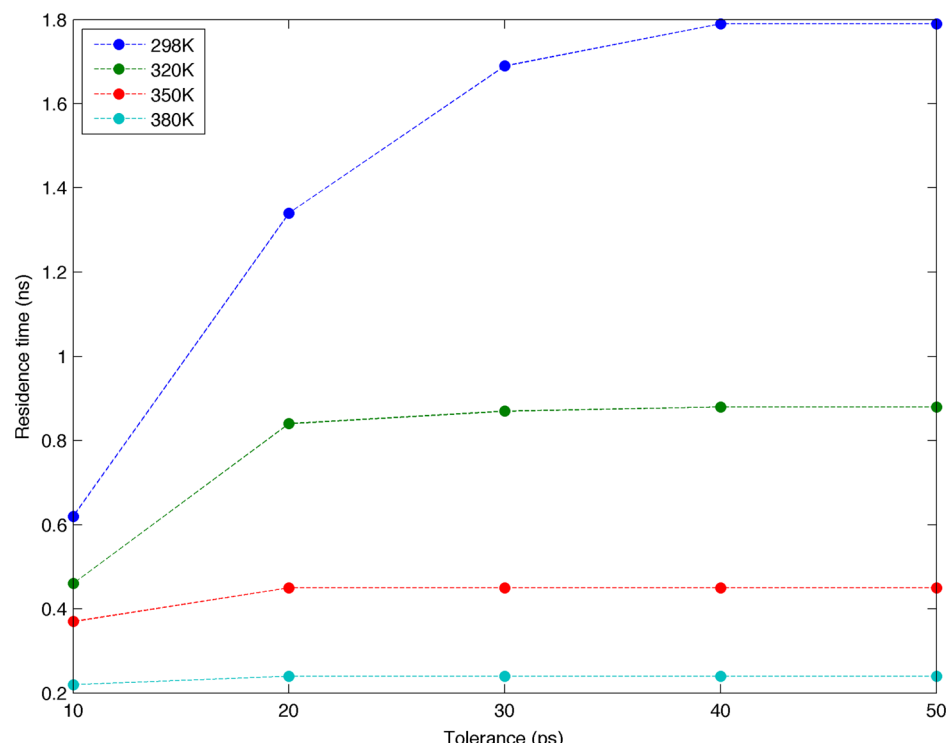
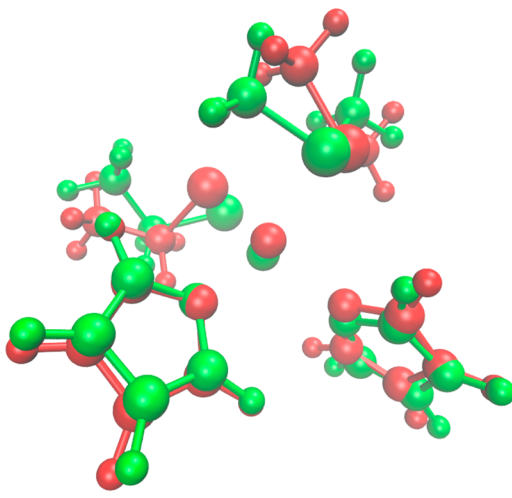


Figure 7. Relationship between computed water residence times in the first solvation shell of Cu^{2+} ion and tolerances for transient water movements in and out of the solvation shell cutoff distance. Calculations performed at various simulation temperatures are color coded.

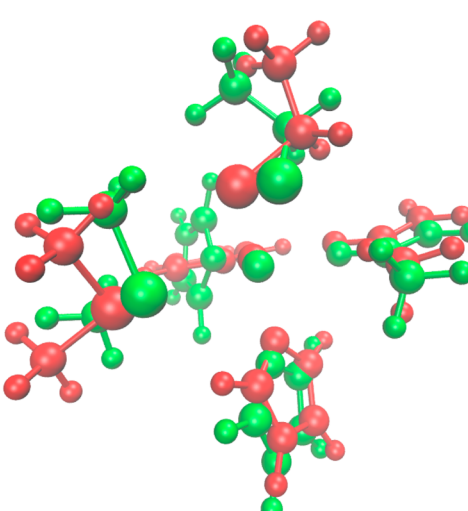
Table 5. Geometries of Optimized T1Cu1 and T1Cu2 Complexes Using DFT, AMOEBA, and AMOEBA-AOM Methods

	T1Cu1			T1Cu2		
	B2LYP-D	AMOEBA-AOM	AMOEBA	B2PLYP-D	AMOEBA-AOM	AMOEBA
Metal–Ligand Bond Length (Å)						
ethyl thiolate	2.20	2.08	2.33	2.12	2.24	2.35
dimethyl sulfide	2.41	2.84	2.41	3.50	2.78	4.13
imidazole 1	2.07	2.32	1.98	2.00	2.36	2.00
imidazole 2	2.20	2.36	1.99	2.02	2.33	2.00
acetamide	—	—	—	2.38	2.49	1.92
Ligand–Metal–Ligand Angle (deg)						
ethyl thiolate–dimethyl sulfide	94.38	105.75	107.99	79.02	90.77	69.42
ethyl thiolate–imidazole 1	148.41	147.40	112.46	123.78	123.38	113.68
ethyl thiolate–imidazole 2	99.54	118.94	115.84	132.95	145.13	113.37
dimethyl sulfide–imidazole 1	90.11	87.37	103.26	91.48	92.34	80.78
dimethyl sulfide–imidazole 2	140.89	93.21	103.84	83.55	88.29	71.48
imidazole 1–imidazole 2	96.44	89.16	112.17	99.86	91.48	110.48
acetamide–ethyl thiolate	—	—	—	107.30	94.63	115.39
acetamide–dimethyl sulfide	—	—	—	172.36	174.55	174.34
acetamide–imidazole 1	—	—	—	88.46	85.30	99.33
acetamide–imidazole 2	—	—	—	88.94	86.86	103.33

T1Cu1



T1Cu2

**Figure 8.** Structures of T1Cu1 and T1Cu2 optimized using B2PLYP-D/cc-pVDZ and AMOEBA-AOM. Colors: QM = red, AMOEBA-AOM = green.**Table 6.** Binding Energies (kcal/mol) of T1Cu1 and T1Cu2 Ligands Computed by MP2, AMOEBA, and AMOEBA-AOM

	T1Cu1			T1Cu2		
	MP2	AMOEBA-AOM	AMOEBA	MP2	AMOEBA-AOM	AMOEBA
ethyl thiolate	-230.0	-265.0	-231.1	-230.8	-219.9	-222.9
dimethyl sulfide	-23.8	-22.0	-31.5	-8.5	-36.0	-14.7
imidazole 1	-43.7	-54.8	-56.9	-43.0	-53.2	-56.9
imidazole 2	-40.5	-48.9	-54.6	-43.0	-47.7	-31.4
acetamide	—	—	—	-20.3	-45.3	-62.1

overlap of optimization results from QM and AMOEBA-AOM is presented in Figure 8. In general, the results computed with the AMOEBA-AOM agree reasonably well with QM structures. The AMOEBA-AOM yields significantly better angular geometry than AMOEBA, which is expected since standard AMOEBA lacks any explicit description of electronic LF effects. It is of interest to point out some discrepancies between the AMOEBA-AOM and QM structures. The geometry obtained

from B2LYP-D optimization shows significant elongation in copper–dimethyl sulfide distance in T1Cu2 compared to T1Cu1. This property is not well described by the AMOEBA-AOM in its current version. A possible explanation is that some of the AOM parameters may be better described by a different function of the metal–ligand distance. The parameters reported were fitted to produce a binding distance of $\sim 2.8 \text{ \AA}$, which is a commonly observed value for

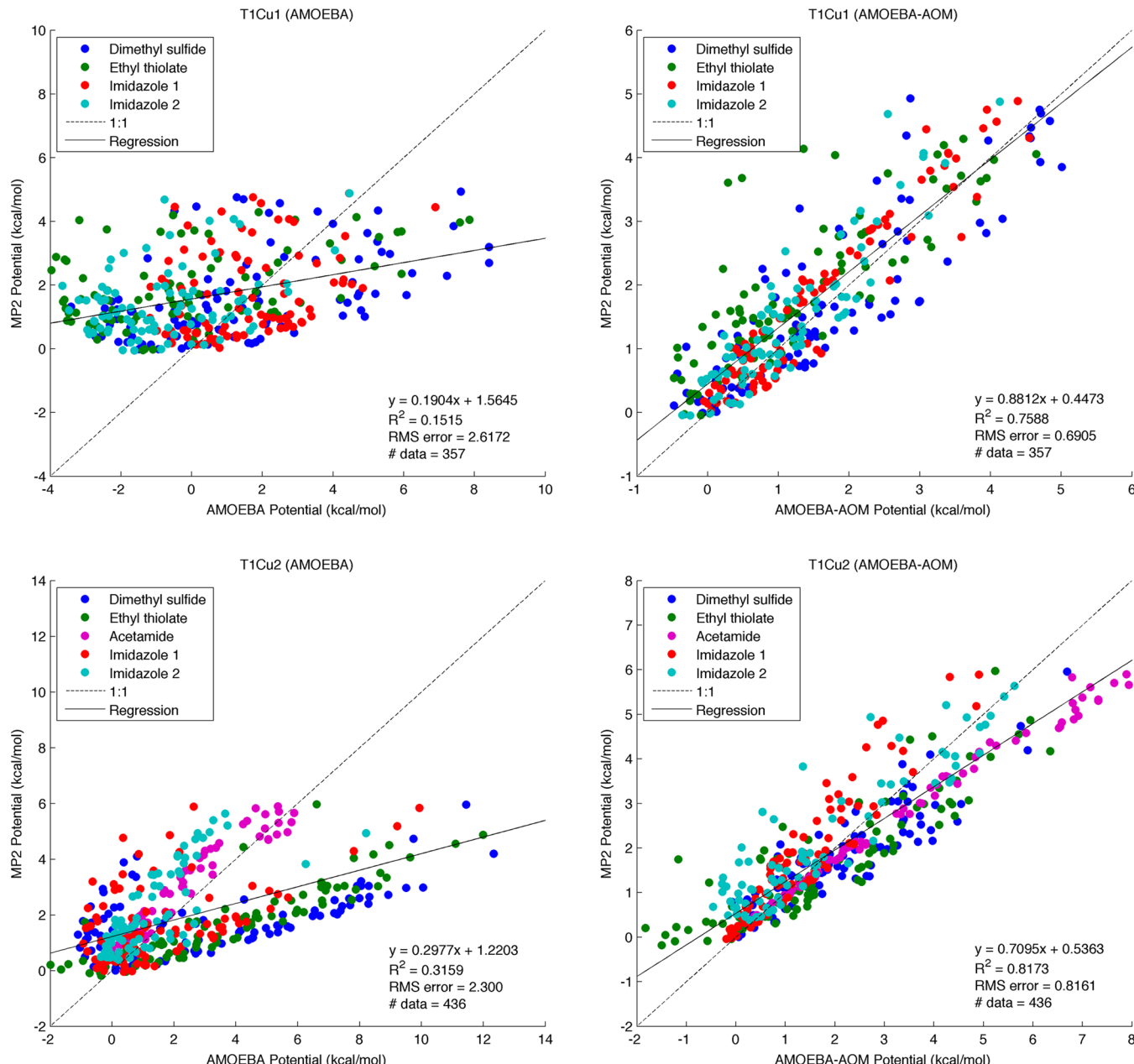


Figure 9. Comparison of QM and MM potentials of random T1Cu1 and T1Cu2 complexes. Results obtained from AMOEBA are plotted on the left column and those computed with the AOM energy terms are on the right. Data point colors represent different sets of structures generated by perturbing a particular type of ligand. Plots of individual ligands can be found in the Supporting Information.

copper-methionine ligation in T1Cu proteins.¹⁰ Furthermore, there is significant deviation from the QM value of the dimethyl sulfide–metal–imidazole 2 angle in T1Cu1. This discrepancy may be a coupled to the difference in binding distances of the dimethyl sulfide ligand.

The binding energies for T1Cu1 and T1Cu2 ligands computed by QM and MM can be found in Table 6. In this context, the AMOEBA-AOM is an improvement over AMOEBA for both the imidazole and acetamide ligands. AMOEBA performs remarkably well for ethyl thiolate, considering the close proximity between two highly charged atoms. However, the AMOEBA-AOM has difficulty in treating some sulfur ligands, especially the dimethyl sulfide ligand in T1Cu2. Nevertheless, the overall energy values are reasonable for this initial implementation of the AMOEBA-AOM. Further refinement of

parameters against a larger set of training complexes should improve the results.

Comparisons of QM and MM potentials of random T1Cu1 and T1Cu2 structures are shown in Figure 9. The addition of the AOM energy term dramatically improves the overall correlation between QM and MM computed potentials. There is a 73% and 64% reduction in RMS error for T1Cu1 and T1Cu2 complexes, respectively. It can be observed that sets of structures with perturbations to sulfur-type ligands results in the largest deviations of the AMOEBA-AOM energies from ab initio potentials.

T1Cu Proteins Simulations. The root-mean-square distances (RMSD) from the initial PDB experimental coordinates for copper-binding side chain and carbonyl atoms are plotted in Figure 10. It is evident that the binding pocket stabilizes after

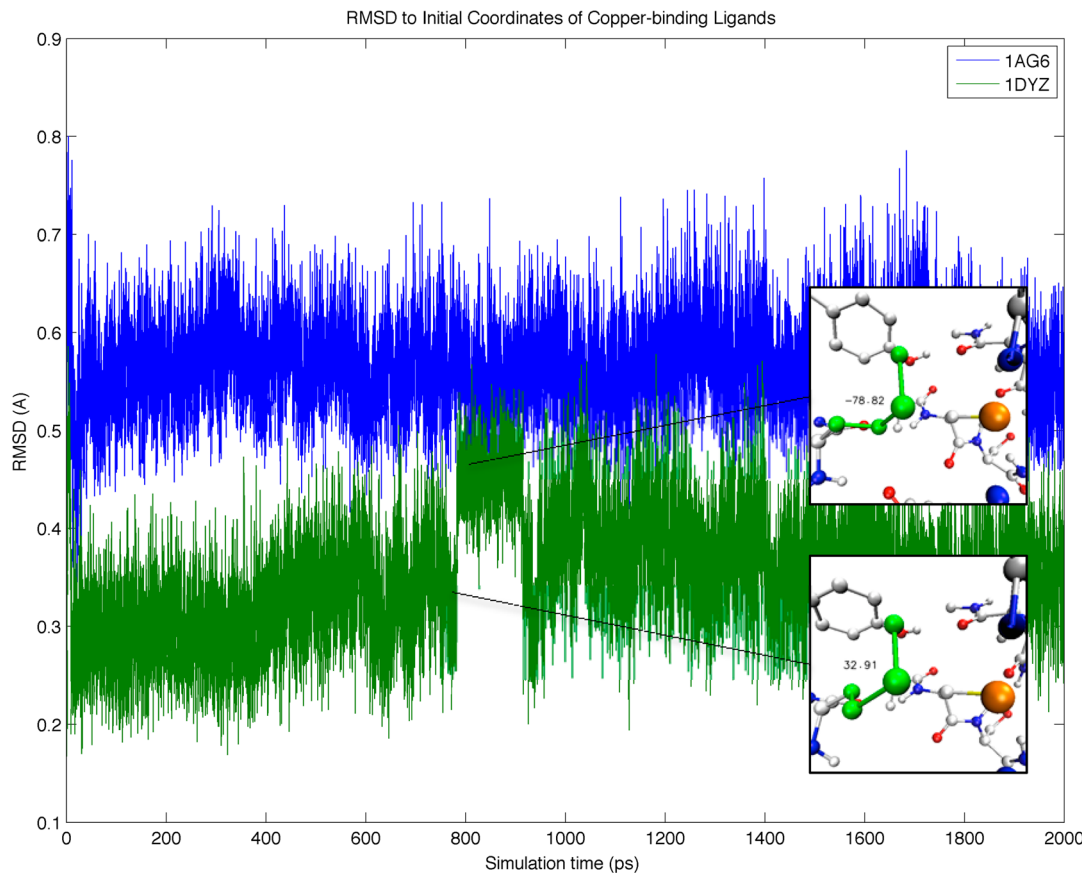


Figure 10. Time evolution of the RMSD to the initial crystallographic coordinates after superposition of copper binding side chain (β -carbon and onward) and backbone carbonyl (both oxygen and carbon) atoms. Figure inserts show snapshots of 1DYZ/MET121 side chain rotation that causes the transition in RMSD plot. Tan sphere represents Cu^{2+} ion.

Table 7. Geometries of Cu^{2+} Binding Sites of 1AG6 and 1DYZ Proteins Obtained From X-ray Crystal Structures and AMOEBA-AOM MD Simulations

1AG6		1DYZ			
experimental	AMOEBA-AOM	experimental	AMOEBA-AOM		
Metal–Ligand Bond Length (Å)					
CYS84	2.15	2.15 ± 0.04	CYS112	2.14	2.49 ± 0.09
MET92	2.88	2.85 ± 0.05	MET121	3.26	2.83 ± 0.05
HIS37	1.96	2.16 ± 0.05	HIS46	2.04	2.13 ± 0.05
HIS87	2.01	2.15 ± 0.05	HIS117	1.99	2.15 ± 0.05
			GLY45	2.72	2.50 ± 0.02
Ligand–Metal–Ligand Angle (deg)					
CYS84–MET92	105.93	95.22 ± 4.38	CYS112–MET121	105.27	103.06 ± 5.43
CYS84–HIS37	129.91	123.67 ± 5.68	CYS112–HIS46	132.56	137.58 ± 5.73
CYS84–HIS87	120.07	133.73 ± 5.80	CYS112–HIS117	121.05	116.49 ± 5.58
MET92–HIS37	87.10	93.50 ± 5.26	MET121–HIS46	73.89	79.73 ± 3.97
MET92–HIS87	102.15	106.15 ± 5.89	MET121–HIS117	88.34	92.47 ± 5.01
HIS37–HIS87	103.04	95.30 ± 4.60	HIS46–HIS117	106.39	105.03 ± 5.66
			GLY45–CYS112	104.10	88.78 ± 5.38
			GLY45–MET121	148.38	166.22 ± 4.27
			GLY45–HIS46	77.77	87.78 ± 4.73
			GLY45–HIS117	86.43	86.92 ± 4.76

initial equilibration. There is a noticeable change in RMSD value at around 0.8 ps for 1DYZ. This is not due to a significant change in direct copper coordination but a rotation of a MET121 side chain dihedral angle illustrated in the figure inserts. The ensemble average geometries of Cu^{2+} binding sites (Table 7) are computed based on the atomic coordinates,

excluding the first 50 ps of each trajectory. In general, the ligation geometry of Cu^{2+} binding sites obtained from MD simulations agrees reasonably well with the X-ray crystal structures. The main difference between simulated and experimental structure is again the methionine binding distance in 1DYZ azurin. The computed average Cu^{2+} -MET121 distance is about

0.4 Å too short, similar to the observations we made for T1Cu2 model complex. This discrepancy has also been found in other computational studies on azurin.^{10,46} Overall, the performance of the AMOEBA-AOM on plastocyanin and azurin is comparable to previously purposed MM models.^{10,46,47}

CONCLUSIONS

The AMOEBA-AOM is an extensible polarizable force field for TM ions that is suitable for studying a variety of TM systems. Its principle advantage over most other AOM-based MM models for TM ion is in the consistent treatment of electrostatics at all distances and explicit description of polarization. This enables the study of ligand association/dissociation and other dynamic events. We have demonstrated that the AMOEBA-AOM provides excellent agreement with QM for a wide range of calculations on aqua Cu²⁺ complexes. It also automatically handles the Jahn-Teller distortion for hexa-aqua Cu²⁺ complex. The computed aqueous Cu²⁺ ligation geometry and water residence time in the first solvation shell are in line with published experimental results. In addition, we have provided evidence for parameter transferability in the context of the T1Cu proteins, yielding reasonable results when compared to gas-phase QM calculations on model complexes and X-ray crystallographic ligation data for complete proteins. Finally, the AMOEBA-AOM is much more efficient than semiempirical or hybrid QM methods, allowing us to perform MD simulations on T1Cu systems investigated in this report that consisting upward of 48 000 atoms.

It should be noted that there are certain limitations to the current AMOEBA-AOM model and the parametrization procedures employed. The AMOEBA-AOM model takes into account the ligand field effect but is not suitable for treating strongly covalent TM systems. In such cases, the AMOEBA-VB approach is perhaps more suitable. In our QM calculations, we have elected to use MP2 method as our model benchmark for parameter fitting. It has been reported that MP2 method for TM ions can be in some cases inferior to DFT results.¹³ However, we noticed that DFT calculations, in our case B3LYP and B2PLYP-D, can converge to dramatically different results for similar structures when they have deviated from the optimum geometry. This represents a challenge because we want to investigate not only the minimum energy structure but also other low-energy conformations. MP2 method was ultimately chosen because of its convergence stability and consistency with normal AMOEBA parametrization routine. In addition, the AOM parameters derived are under-determined. A larger QM benchmark set should ideally be used to improve the transferability of the model parameters.

There are other areas of improvements that can be made to the AMOEBA-AOM formulation. First is a better method of handling the elongation of the dimethyl sulfide/methionine ligand as described earlier. A possible solution is by applying functional forms for ϵ_{AOM} different from this initial iteration. Alternatively, a coupling of metal-ligand bonding to the L-M-L angle similar to the strategy of AMOEBA-VB⁴⁰ can be explored. A second aspect of the AMOEBA-AOM that can be improved is its accuracy in describing sulfur ligand binding energies. The Morse bonding term can be replaced with a different, more flexible, functional form. An interesting candidate is to reintroduce the buffered 14-7 vdW potential used by the standard AMOEBA force field for sulfur ligands since it shows remarkable agreement with QM energies. It should be noted that previous efforts to model the LF effects have been largely

focused on geometries. We believe that the accurate description of ligand binding energies is also an important aspect of any MM model, especially if one wants to study ligand exchanges, vibrational frequencies, and other dynamic events.

In addition to making improvements to the AMOEBA-AOM as outlined above and continuing refinement of the AMOEBA-AOM parameters, it would be interesting to apply the AMOEBA-AOM to other copper centers and produce a complete set of parameters for all amino acid ligands. One intriguing area for study is to investigation of conformational changes in T1Cu proteins between their oxidized and reduced forms. Indeed, the two forms have different binding partners at the metal center. Since Cu⁺ has a d¹⁰ configuration, it can be treated in similar fashion to Zn²⁺ as we have demonstrated,⁴⁰ albeit with a different formal charge assignment. This work is planned for the near future.

ASSOCIATED CONTENT

Supporting Information

The AMOEBA parameters for the ligands were obtained following published protocols. AMOEBA parameter values, as well as figures showing results for randomly perturbed T1Cu1 and T1Cu2 clusters, are provided as supporting information. This material is available free of charge via the Internet at <http://pubs.acs.org>.

AUTHOR INFORMATION

Corresponding Author

*E-mail: ponder@dasher.wustl.edu

Notes

The authors declare no competing financial interest.

ACKNOWLEDGMENTS

We would like to thank the National Science Foundation (Award CHE1152823) and National Institutes of Health (R01 GM106137) for their generous support of this research via grants to J.W.P.

REFERENCES

- (1) Lippard, S. J.; Berg, J. M. *Principles of Bioinorganic Chemistry*; University Science Books: Herndon, VA, 1994.
- (2) Holm, R. H.; Kennepohl, P.; Solomon, E. I. *Chem. Rev.* **1996**, *96*, 2239–2314.
- (3) *Bioorganometallics: Biomolecules, Labeling, Medicine*; Jaouen, G., Ed. Wiley-VCH: Weinheim, 2006.
- (4) *Biological Inorganic Chemistry: Structure and Reactivity*, 1st ed.; Gray, H. B.; Stiefel, E. I.; Valentine, J. S.; Bertini, I., Eds.; University Science Books: Herndon, VA, 2006.
- (5) Crabtree, R. H. *The Organometallic Chemistry of the Transition Metals*, 5 ed.; John Wiley & Sons, Inc.: Hoboken, NJ, 2009.
- (6) Hartinger, C. G.; Dyson, P. J. *Chem. Soc. Rev.* **2009**, *38*, 391.
- (7) Hillard, E. A.; Jaouen, G. *Organometallics* **2011**, *30*, 20–27.
- (8) Comba, P.; Hambley, T. W.; Martin, B. *Molecular Modeling of Inorganic Compounds*; Wiley-VCH: Weinheim, 2009.
- (9) *Modeling of Molecular Properties*; Comba, P., Ed. Wiley-VCH: Weinheim, 2011.
- (10) Deeth, R. J.; Anastasi, A.; Diedrich, C.; Randell, K. *Coord. Chem. Rev.* **2009**, *293*, 795–816.
- (11) Constable, E. G.; Gerloch, M. *Transition Metal Chemistry*; VCH Verlagsgesellschaft mbH: Weinheim, 1997.
- (12) Jean, Y. *Molecular Orbitals of Transition Metal Complexes*; Oxford University Press: Oxford, 2005.
- (13) Harvey, J. N. *Annu. Rep. Prog. Chem., Sect. C: Phys. Chem.* **2006**, *102*, 203.

- (14) Cramer, C. J.; Truhlar, D. G. *Phys. Chem. Chem. Phys.* **2009**, *11*, 10757.
- (15) Winget, P.; Sel uki, C.; Horn, A. H. C.; Martin, B.; Clark, T. *Theor. Chem. Acc.* **2003**, *110*, 254–266.
- (16) Bredow, T.; Jug, K. *Theor. Chem. Acc.* **2005**, *113*, 1–14.
- (17) Friesner, R. A.; Guallar, V. *Annu. Rev. Phys. Chem.* **2005**, *56*, 389–427.
- (18) Ochsenfeld, C.; White, C. A.; Head-Gordon, M. *J. Chem. Phys.* **1998**, *109*, 1663–1669.
- (19) Babu, K.; Gadre, S. R. *J. Comput. Chem.* **2003**, 484–495.
- (20) Nielson, K. D.; van Duin, A. C. T.; Oxaard, J.; Deng, W.-Q.; Goddard, W. A. *J. Phys. Chem. A* **2005**, *109*, 493–499.
- (21) van Duin, A. C. T.; Bryantsev, V. S.; Diallo, M. S.; Goddard, W. A.; Rahaman, O.; Doren, D. J.; Raymand, D.; Hermansson, K. *J. Phys. Chem. A* **2010**, *114*, 9507–9514.
- (22) Pauling, L. *Phys. Rev.* **1938**, *54*, 899–904.
- (23) Pauling, L. *Proc. R. Soc. London, Ser. A* **1949**, *196*, 343–362.
- (24) Pauling, L. *Proc. Natl. Acad. Sci. U.S.A.* **1976**, *73*, 1403–1405.
- (25) Weinhold, F.; Landis, C. R. *Valency and bonding*; Cambridge University Press: Cambridge, 2005.
- (26) Schäffer, C. E.; Jørgensen, C. K. *Mol. Phys.* **1965**, *9*, 401–412.
- (27) Landis, C.; Cleveland, T. *J. Am. Chem. Soc.* **1993**, *115*, 4201–4209.
- (28) Cleveland, T.; Landis, C. R. *J. Am. Chem. Soc.* **1996**, *118*, 6020–6030.
- (29) Landis, C.; Cleveland, T. *J. Am. Chem. Soc.* **1998**, *120*, 2641–2649.
- (30) Firman, T. K.; Landis, C. R. *J. Am. Chem. Soc.* **2001**, *123*, 11728–11742.
- (31) Deeth, R. J.; Foulis, D. L. *Phys. Chem. Chem. Phys.* **2002**, *4*, 4292–4297.
- (32) Deeth, R. J. *Faraday Disc.* **2003**, *124*, 379.
- (33) Deeth, R. J.; Fey, N.; Williams-Hubbard, B. *J. Comput. Chem.* **2004**, *26*, 123–130.
- (34) Carlsson, A. E. *Phys. Rev. Lett.* **1998**, *81*, 477–480.
- (35) Carlsson, A. E.; Zapata, S. *Biophys. J.* **2001**, *81*, 1–10.
- (36) Zapata, S.; Carlsson, A. *Phys. Rev. B* **2002**, *66*, 174106.
- (37) Carlsson, H.; Haukka, M.; Bousseksou, A.; Latour, J.-M.; Nordlander, E. *Inorg. Chem.* **2004**, *43*, 8252–8262.
- (38) Ponder, J. W.; Case, D. A. *Adv. Protein Chem.* **2003**, *66*, 27–85.
- (39) Ren, P.; Ponder, J. W. *J. Comput. Chem.* **2002**, *23*, 1497–1506.
- (40) Xiang, J. Y.; Ponder, J. W. *J. Comput. Chem.* **2012**, *34*, 739–749.
- (41) Deeth, R. J.; Hearnshaw, L. J. A. *Dalton Trans.* **2005**, *22*, 3638.
- (42) Deeth, R. J.; Hearnshaw, L. J. A. *Dalton Trans.* **2006**, *8*, 1092.
- (43) Bentz, A.; Comba, P.; Deeth, R. J.; Kerscher, M.; Seibold, B.; Wadeohl, H. *Inorg. Chem.* **2008**, *47*, 9518–9527.
- (44) Xue, Y.; Okvist, M.; Hansson, O.; Young, S. *Protein Sci.* **1998**, *7*, 2099–2105.
- (45) Dodd, D. E.; Abraham, D. H. L.; Eady, D. R.; Hasnain, S. S. *Acta Crystallogr. B* **2000**, *D56*, 690–696, DOI: 10.1107/S0907444900003309.
- (46) Comba, P.; Remenyi, R. *J. Comput. Chem.* **2002**, *23*, 697–705.
- (47) De Rienzo, F.; Gabdoulline, R. R.; Wade, R. C.; Sola, M.; Menziani, M. C. *Cell. Mol. Life Sci.* **2004**, *61*, 1123–1142.
- (48) Deeth, R. J. *Inorg. Chem.* **2007**, *46*, 4492–4503.
- (49) Ren, P.; Ponder, J. W. *J. Phys. Chem. B* **2003**, *107*, 5933–5947.
- (50) Ren, P.; Wu, C.; Ponder, J. W. *J. Chem. Theory Comput.* **2011**, *7*, 3143–3161.
- (51) Halgren, T. A. *J. Am. Chem. Soc.* **1992**, *114*, 7827–7843.
- (52) Stone, A. J. *The Theory of Intermolecular Forces*; Oxford University Press: Oxford, 1997.
- (53) Thole, B. T. *Chem. Phys.* **1981**, *59*, 341–350.
- (54) Figgis, B. N.; Hitchman, M. A. *Ligand Field Theory And Its Applications*; Wiley-VCH: New York, 2000.
- (55) Rose, M. *Elementary Theory Of Angular Momentum*; Wiley: New York, 1957.
- (56) Frisch, M. J.; Trucks, G. W.; Schlegel, H. B.; Scuseria, G. E.; Robb, M. A.; Cheeseman, J. R.; Scalmani, G.; Barone, V.; Mennucci, B.; Petersson, G. A.; Nakatsuji, H.; Caricato, M.; Li, X.; Hratchian, H. P.; Izmaylov, A. F.; Bloino, J.; Zheng, G.; Sonnenberg, J. L.; Hada, M.; Ehara, M.; Toyota, K.; Fukuda, R.; Hasegawa, J.; Ishida, M.; Nakajima, T.; Honda, Y.; Kitao, O.; Nakai, N.; Vreven, T.; Montgomery, J. A., Jr.; Peralta, J. E.; Ogliaro, F.; Bearpark, M.; Heyd, J. J.; Brothers, E.; Kudin, K. N.; Staroverov, V. N.; Kobayashi, R.; Normand, J.; Ragahavachari, K.; Rendell, A.; Burant, J. C.; Iyengar, S. S.; Tomasi, J.; Cossi, M.; Rega, N.; Millam, J. M.; Klene, M.; Knox, J. E.; Cross, J. B.; Bakken, V.; Adamo, C.; Jaramillo, J.; Gomperts, R.; Stratmann, R. E.; Yazayev, O.; Austin, A. J.; Cammi, R.; Pomelli, C.; Ochterski, J. W.; Martin, R. L.; Morokuma, K.; Zakrzewski, V. G.; Voth, G. A.; Salvador, P.; Dannenberg, J. J.; Dapprich, S.; Daniels, A. D.; Farkas, Ö.; Foresman, J. B.; Ortiz, J.; Cioslowski, J.; Fox, D. J. *Gaussian 09*, revision A.2; Gaussian, Inc.: Wallingford, CT2009.
- (57) Lee, C.; Yang, W.; Parr, R. *Phys. Rev. B Condens. Matter* **1988**, *37*, 785–789.
- (58) Becke, A. D. *J. Chem. Phys.* **1993**, *98*, 5648–5652.
- (59) Binning, R. C.; Curtiss, L. A. *J. Comput. Chem.* **1990**, *11*, 1206–1216.
- (60) Head-Gordon, M.; Pople, J. A.; Frisch, M. *J. Chem. Phys. Lett.* **1988**, *153*, 503–506.
- (61) Dunning, T. *J. Chem. Phys.* **1989**, *90*, 1007–1023.
- (62) Balabanov, N. B.; Peterson, K. A. *J. Chem. Phys.* **2005**, *123*, 064107.
- (63) Rabuck, A. D.; Scuseria, G. E. *J. Chem. Phys.* **1999**, *110*, 695–700.
- (64) Grimme, S. *J. Chem. Phys.* **2006**, *27*, 1787–1799.
- (65) Schwabe, T.; Grimme, S. *Phys. Chem. Chem. Phys.* **2007**, *9*, 3397–3406.
- (66) Nyman, T. M. *J. Chem. Phys.* **2000**, *112*, 6152–6160.
- (67) Toukmaji, A.; Sagui, C.; Board, J.; Darden, T. *J. Chem. Phys.* **2000**, *113*, 10913.
- (68) Ponder, J. W.; Wu, C.; Ren, P.; Pande, V. S.; Chodera, J. D.; Schnieders, M. J.; Haque, I.; Mobley, D. L.; Lambrecht, D. S.; DiStasio, R. A., Jr.; Head-Gordon, M.; Clark, G. N. I.; Johnson, M. E.; Head-Gordon, T. *J. Phys. Chem. B* **2010**, *114*, 2549–2564.
- (69) Uranga, J.; Mikulkis, P.; Genheden, S.; Ryde, U. *Comput. Theor. Chem.* **2012**, *1000*, 75–84.
- (70) Helm, L.; Merbach, A. E. *Coord. Chem. Rev.* **1999**, *187*, 151–181.
- (71) Pasquarello, A.; Petri, I.; Salmon, P. S.; Parisel, O.; Car, R.; Toth, E.; Powell, D. D.; Fischer, H. E.; Helm, L.; Merbach, A. E. *Science* **2001**, *291*, 856–859.
- (72) Ohtaki, H. *Monatsh. Chem.* **2001**, *132*, 1237–1268.
- (73) de Almeida, K. J.; Murugan, N. A.; Rinkevicius, Z.; Hugosson, H. W.; Vahtras, O.; Ågren, H.; Cesar, A. *Phys. Chem. Chem. Phys.* **2009**, *11*, 508.
- (74) Rode, B. M.; Schwenk, C. F.; Hofer, T. S.; Randolph, B. R. *Coord. Chem. Rev.* **2005**, *249*, 2993–3006.
- (75) Kumar, R.; Keyes, T. *J. Am. Chem. Soc.* **2011**, *133*, 9441–9450.
- (76) Frank, P.; Benfatto, M.; Szilagyi, R. K.; D'Angelo, P.; Longa, S. D.; Hodgson, K. O. *Inorg. Chem.* **2005**, *44*, 1922–1933.
- (77) Blumberger, J. *J. Am. Chem. Soc.* **2008**, *130*, 16065–16068.
- (78) Chaboy, J.; Muñoz-Páez, A.; Merkling, P. J.; Sánchez Marcos, E. *J. Chem. Phys.* **2006**, *124*, 064509.
- (79) Swift, T. J.; Connick, R. E. *J. Chem. Phys.* **1962**, *37*, 307–320.
- (80) Ohtaki, H.; Radnai, T. *Chem. Rev.* **1993**, *93*, 1157–1204.
- (81) Salmon, P. S.; Bellissent-Funel, M.-C.; Herdman, G. J. *J. Phys.: Condens. Matter* **1990**, *2*, 4297.
- (82) Neilson, G. W.; Newsome, J. R.; Sandström, M. *J. Chem. Soc., Faraday Trans. 2* **1981**, *77*, 1245–1256.
- (83) Sham, T.; Hastings, J.; Perlman, M. *Chem. Phys. Lett.* **1981**, *83*, 391–396.
- (84) Beagley, B.; Eriksson, A.; Lindgren, J.; Persson, I.; Pettersson, L. G. M.; Sandstrom, M.; Wahlgren, U.; White, E. W. *J. Phys.: Condens. Matter* **1989**, *1*, 2395–2408.
- (85) Amira, S.; Spångberg, D.; Hermansson, K. *Phys. Chem. Chem. Phys.* **2005**, *7*, 2874.
- (86) Schwenk, C. F.; Rode, B. M. *J. Chem. Phys.* **2003**, *119*, 9523.
- (87) Moin, S. T.; Hofer, T. S.; Weiss, A. K. H.; Rode, B. M. *J. Chem. Phys.* **2013**, *139*, 014503.